Thermochemical Storage of Solar Energy via Fluidised Bed Calcium Looping – Relationship Between Sorbent Properties and Process Performances under Variable Operating Conditions

Giusy Marotta[1,2,*], Shouzhuang Li[3,4], Claudio Tregambi[5,2], Francesca Di Lauro[6,2], Marco Balsamo[1], Fabio Montagnaro[1,2,*], Mika Järvinen[3], Piero Salatino[6], Roberto Solimene[2]

[1]Department of Chemical Sciences, University of Naples Federico II, 80126 Naples, Italy
[2]Institute of Sciences and Technologies for Sustainable Energy and Mobility, National Research Council, 80125 Naples, Italy
[3]Department of Energy and Mechanical Engineering, Aalto University, 02150 Espoo, Finland
[4]State Key Laboratory of Heavy Oil Processing, China University of Petroleum, 102249 Beijing, China
[5]Department of Engineering, University of Sannio, 82100 Benevento, Italy
[6]Department of Chemical, Materials and Industrial Production Engineering, University of Naples Federico II, 80125 Naples, Italy

Abstract. Thermochemical storage of solar energy via fluidised bed calcium looping is emerging as a promising technology. In this work, the combined effect of carbonation and calcination temperatures on sorbent deactivation and energy storage in a directly irradiated fluidised bed reactor was assessed. Experiments were carried out over 10 calcination–carbonation cycles. Results show that increasing calcination temperature accelerates sorbent deactivation, whereas carbonation temperature plays a minor role. A larger temperature difference between calcination and carbonation enhances particle size reduction due to thermal and mechanical stresses. A compensation effect between sorbent reactivity and the process temperature gradient on energy storage density was observed. At higher cycle numbers, maximum energy storage density was achieved at T_{carb} = 600°C and T_{calc} = 800°C, identifying these conditions as optimal for material performance. In terms of particle comminution, it emerges as one of the key phenomena governing the long-term evolution of the bed inventory in solar-driven calcium looping for thermochemical energy storage, with potential implications on fluid-dynamic stability, elutriation, and the effective sorbent residence time.

1. Introduction and aim of the work

Anthropogenic CO_2 emissions represent the primary driver of global climate change: in 2025, they reached approximately 38.4 Gt, with atmospheric CO_2 concentration of about 427 ppm [1]. In this context, the rapid implementation of decarbonisation strategies, including CO_2 capture, is essential to limit rising emissions. Calcium Looping (CaL) is a promising post-combustion CO_2 capture technology (currently, at TRL 6–7 on average) that can be integrated into combustion and gasification plants [2]. CaL consists of the cyclic carbonation and calcination of $CaCO_3$, typically carried out in two interconnected Fluidised Bed (FB) reactors [3]. During carbonation, CO_2-rich flue gas reacts with CaO at 600–700°C to form $CaCO_3$. The solid is transferred to a second reactor and calcined at 800–900°C, releasing concentrated CO_2 flue gas and regenerating the CaO sorbent [4]. Calcination is an endothermic process requiring high temperatures which can be directly supplied by Concentrated Solar Power (CSP) systems, thus enhancing the process sustainability and environmental relevance. CaL-CSP systems have been widely studied for ThermoChemical Energy Storage (TCES) due to their high reaction heat and low-cost sorbent material [5]. The main drawback of CaL is the sorbent particles deactivation over cycles due to sintering and pore plugging, which reduce CO_2 capture and energy storage performance [6]. This depends on material impurities, CO_2 partial pressure, temperatures of carbonation (T_{carb}) and calcination (T_{calc}), and particle comminution. In this work, the reactivity of the sorbent is evaluated in a FB reactor coupled with a concentrated solar radiation simulator [7]. The effect of T_{carb} and T_{calc} on material performance is investigated, with emphasis on the role of comminution of sorbent particles.

2. Experimental campaign

2.1. Materials

* Corresponding authors: fabio.montagnaro@unina.it; giusy.marotta@unina.it

The FB inventory consisted of inert sand and reactive sorbent. Silica sand was used as inert material (particle density: 2600 kg/m^3; size: 850–1000 µm). A natural Italian limestone (98.5%$_{wt}$ $CaCO_3$) was used as sorbent (particle density: 2400 kg/m^3; size: 420–590 µm), allowing easy separation from sand after each test.

2.2. Experimental conditions

Figure 1 depicts the experimental set-up adopted for CaL tests [6,7]. It consists of three sections: bubbling fluidized bed, wind-box and conical freeboard, which is closed by a ceramic glass optical window. Concentrated solar radiation is simulated by three short-arch Xe-lamps (4 kW$_{el}$ each) coupled with elliptical reflectors. An electric heating system – comprising a gas preheater and radiant heaters – is used during non-solar operation.

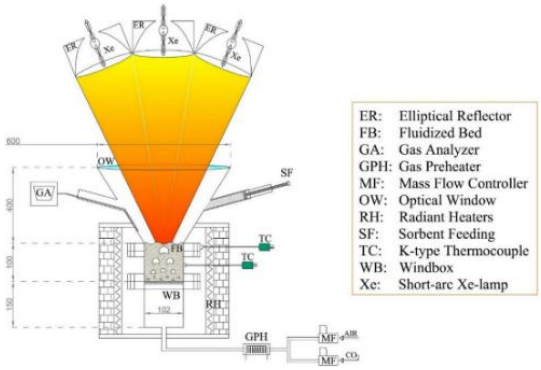

Figure 1. Layout of the concentrated solar FB reactor.

The experimental campaign investigated carbonation and calcination at 600°C, 650°C, 700°C, and 800°C, 850°C, 900°C, respectively, for ten reaction cycles (*N*). Carbonation was performed with CO_2 concentration in the inlet gas of 10%$_v$; while calcination was carried out using air as the fluidising gas. The fluidisation velocity was set at 0.6 m/s for all conditions. Carbonated particles recovered after cycles $N = 1$, 4, 7, and 10 were sieved into size fractions of 300–420, 200–300, and 100–200 µm to determine the Particle Size Distribution (PSD). Calcined particles from cycles 0 and 8 were collected for N_2 porosimetry analyses. The data were processed to evaluate the specific surface area, total pore volume, and pore size distribution.

2.3. Data analysis

The collected carbonated samples (after a given cycle *N*) were analysed to determine the carbonation degree following the procedure described in Di Lauro et al. [6]. After heating the sample (once FB-carbonated for *N* cycles) at 950°C in a muffle furnace, the carbonation degree $\bar{X}_{Ca}(N)$ was calculated using Eq. (1) as the ratio between the moles of CO_2 released (i.e., moles of $CaCO_3$ formed upon carbonation) and the total moles of CaO:

$$\bar{X}_{Ca}(N) = \frac{(m_b^N - m_a^N)}{m_a^N x_{CaO}} \frac{M_{CaO}}{M_{CO_2}} \quad (1)$$

where m_b^N and m_a^N stand for the sample mass before and after heating in the muffle furnace, respectively; x_{CaO} is the CaO mass fraction in the parent sorbent; M_{CaO} and M_{CO_2} are the molar mass of CaO and CO_2, respectively. The energy storage density (E_{SD}) [MJ/m^3] at cycle *N* was calculated using Eq. (2), where $\Delta_r H$ is the reaction heat (standard value: 178 kJ/mol) at the corresponding carbonation temperature, ρ_{bulk} is the bulk density of limestone (1385 kg/m^3) and x_{CaCO_3} is the mass fraction of $CaCO_3$ in the feedstock limestone, while $\overline{C}_p$ is an average value for the specific heat capacity of $CaCO_3$ (1 kJ/(kg °C)), and M_{CaCO_3} is the molar mass of calcium carbonate. Finally, in Eq. (2), $X_{Ca,N}^{av}$ is the carbonation degree averaged up to the considered reaction cycle *N* (Eq. (3)).

$$E_{SD}(N) = \Delta_r H X_{Ca,N}^{av} \frac{\rho_{bulk}\, x_{CaCO_3}}{M_{CaCO_3}} + \rho_{bulk}\, \overline{C}_p (T_{calc} - T_{carb}) \quad (2)$$

$$X_{Ca,N}^{av} = \frac{\sum_{N=1}^{N} \bar{X}_{Ca}(N)}{N} \quad (3)$$

3. Results and related discussion

Figure 2 reports the effect of calcination and carbonation temperatures on the sorbent carbonation degree, whose trend is decreasing along *N* due to the progressive particle deactivation by thermal sintering.

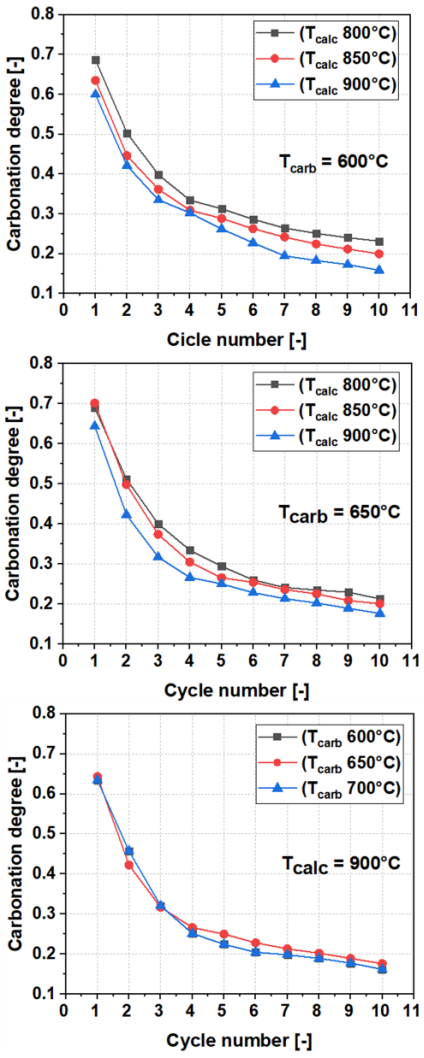

Figure 2. Evolution of carbonation degree (Eq. (1)) upon iterated CaL cycles for different T_{carb} and T_{calc}.

$\bar{X}_{Ca}$ drops markedly during the first five cycles, followed by a more gradual decrease thereafter. For example, at T_{calc} = 800°C and T_{carb} = 600°C, it decreases from 0.69 (N = 1) to 0.31 (N = 5) and approaches 0.23 for N = 10. This can be ascribed to the agglomeration of CaO grains, to form a rigid and interconnected structure, further protected by an outer $CaCO_3$ layer, which limits further sintering as N increases on and on. However, agglomeration inevitably reduces porosity and specific surface area, enhancing CaO deactivation. These effects intensify with increasing T_{calc}, while rising T_{carb} has a marginal role.

The porosimetry analysis and specific surface area of the tests conducted at fixed T_{carb} (650°C) and T_{calc} of 800°C and 900°C are shown in Figure 3 and Table 1.

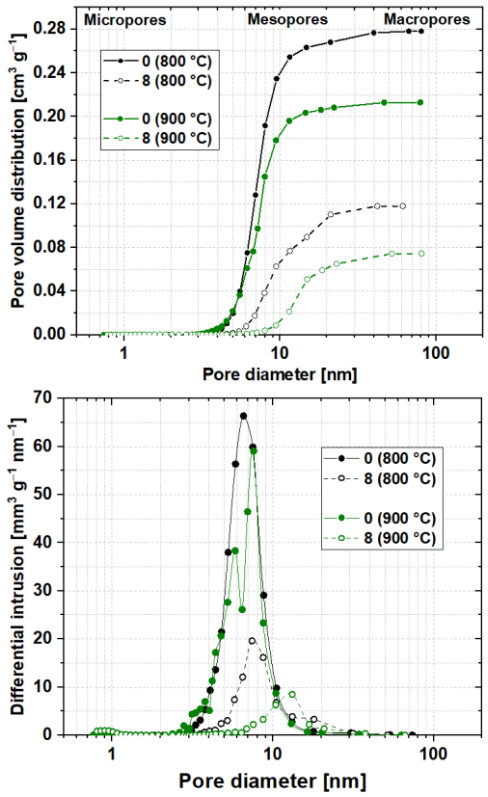

Figure 3. Cumulative specific pore volume (up) and differential intrusion curves (down) vs. pore diameter. Data refer to samples at different cycle numbers and calcination temperatures (keeping T_{carb} = 650 °C).

For each process condition, the specific surface area and total porosity after the eighth calcination are significantly lower than those after the initial calcination (labelled as N = 0). As T_{calc} increases, the samples show a relevant reduction in both specific surface area and total porosity. Furthermore, differential intrusion data reveal that higher calcination temperatures promote pore coalescence, leading to particle sintering. Specifically, increasing T_{calc} from 800°C to 900°C shifts the pore size distribution peak from ~7.5 nm to ~15 nm, an effect more pronounced after the eighth calcination. These results strengthen the view of loss in reactive porosity when calcination temperature (or reaction cycle) increases.

Table 1. Porosimetry data of samples in Figure 2.

$T_{calc} - N$	Specific surface [m²/g]	Total pore volume [cm³/g]
800°C – 0	21.9	0.27
800°C – 8	6.8	0.11
900°C – 0	18.6	0.20
900°C – 8	3.7	0.07

Now the results concerning particle comminution analysis will be presented. It is highlighted that, starting from a parent limestone size range of 420–590 µm, particle fragmentation predominantly occurs within the 300–420 µm fraction. Figure 3 reports the average mass fraction of particles in this range and the mean Sauter diameter, as a function of N and the temperature difference ΔT (i.e., T_{calc}–T_{carb}).

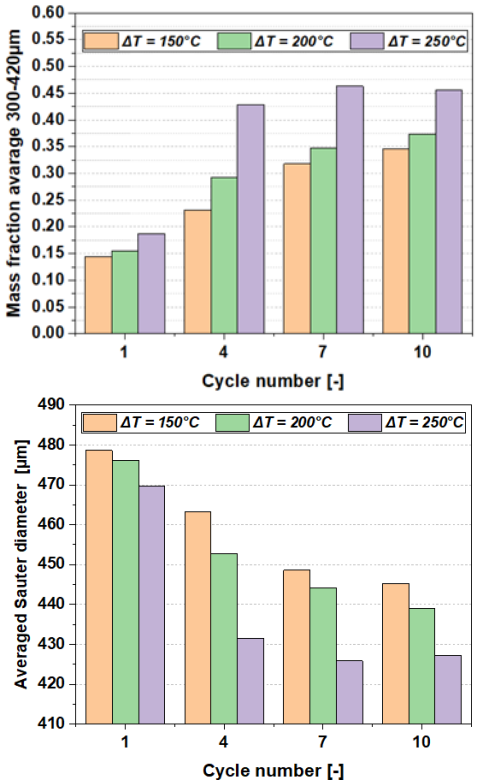

Figure 4. Mass fraction of 300–420 µm particles (up), and averaged Sauter diameter for the whole PSD (down), for samples collected upon iterated cycles of calcination/carbonation; data parametric in the temperature difference between carbonation and calcination.

As N increases, the 300–420 µm mass fraction rises, while the average Sauter diameter decreases for all the investigated conditions. Fragmentation is most severe during the first four cycles and weakens thereafter. This behaviour is attributed to a combination of different factors: i) thermal shock experienced by carbonated particles upon entering the calcination reactor; ii) attrition mechanisms, which initially smooth particle asperities and subsequently promote continuous material removal

through mechanical stresses; iii) rapid CO_2 release at higher calcination temperatures. More in detail, the PSD mean Sauter diameter decreases from ca. 478 to 445 µm when N increases from 1 to 10 (ΔT = 150°C), and from ca. 470 to 425 µm when N increases from 1 to 10 (ΔT = 250°C). A relevant feature is that, the higher the thermal gap suffered by the particles upon cycling (ΔT), the lower the mean diameter, namely the larger the extent of particle comminution. The ~10% reduction in Sauter diameter measured over 10 cycles, coupled with the progressive enrichment of the 300–420 µm fraction, could perturb the fluid-dynamic regime of the bed (e.g., minimum fluidisation velocity, segregation patterns) and enhance fines elutriation, thereby establishing comminution as a mechanism that, alongside chemical deactivation, influences the operability window of solar-assisted CaL at industrial scale.

Figure 5 presents the effect of calcination and carbonation temperatures on energy storage density for experiments at T_{carb} = 600–650°C and T_{calc} = 800–900°C.

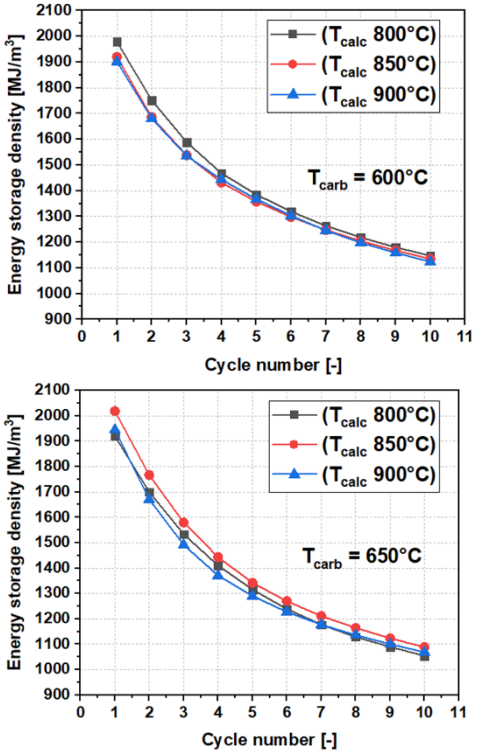

Figure 5. Effect of carbonation and calcination temperatures on energy story density (Eq. (2)).

E_{SD} decreases with N, consistent with the trend observed for the carbonation degree. Overall, it declines from 1900–2020 MJ/m^3 at N = 1 to 1050–1150 MJ/m^3 at N = 10. Energy storage density depends on both $\bar{X}_{Ca}$ and ΔT; therefore, lower $\bar{X}_{Ca}$ values (which tend to reduce E_{SD}) can be compensated by higher ΔT (which increases it). Indeed, for all plots of Figure 5, the curves are nearly overlapping due to a compensation effect between lower ΔT and higher reactivity. In detail, while a lower T_{calc} increases $\bar{X}_{Ca}$ (thus increasing E_{SD}), it simultaneously reduces ΔT, leading to a decrease in E_{SD}.

4. Conclusions

This study investigates the combined effect of carbonation and calcination temperatures in a solar-assisted CaL process, using a directly irradiated FB reactor coupled with a concentrated solar radiation simulator. Results show a rapid decrease in carbonation degree during the initial cycles, driven by sorbent sintering, as indicated by the reduction in specific surface area and porosity. The decline is amplified at higher calcination temperatures. It was also observed that a larger temperature difference between carbonation and calcination promotes greater particle size reduction, driven by increased thermal stresses. Energy storage data were evaluated across different process conditions, revealing a compensation effect between sorbent reactivity and ΔT.

In terms of particle comminution, it can be regarded as an intrinsic, and unavoidable, feature of solar-assisted CaL operation: its coupling with thermal shocks, attrition, and CO_2-release-driven mechanical stresses ultimately co-determines, together with sorbent chemical deactivation, the achievable energy storage density and the long-term operability of the technology.

Acknowledgement

Part of this work was funded by Walter Ahlström Foundation, Grant number: 20230030, supported by the School of Engineering, Aalto University, Finland. This work was carried out within the Research Project of Relevant National Interest (PRIN) P202224CPL, funded by the European Union – Next Generation EU.

References

[1] International Energy Agency, Global Energy Review (2026). https://www.iea.org/reports/global-energy-review-2026/co2-emissions

[2] Tregambi, C., Bareschino, P., Hanak, D.P., Montagnaro, F., Pepe, F., Mancusi, E. (2022) Modelling of an integrated process for atmospheric carbon dioxide capture and methanation. *J. Clean. Prod.*, 356, 131827.

[3] Arias, B., Diego, M.E., Méndez, A., Alonso, M., Abanades, J.C. (2018) Calcium looping performance under extreme oxy-fuel combustion conditions in the calciner. *Fuel*, 222, 711–717.

[4] Chen, J., Duan, L., Sun, Z. (2020) Review on the development of sorbents for calcium looping. *Energy Fuels*, 34, 7806–7836.

[5] Tregambi, C., Montagnaro, F., Salatino, P., Solimene, R. (2015) A model of integrated calcium looping for CO_2 capture and concentrated solar power. *Sol. Energy*, 120, 208–220.

[6] Di Lauro, F., Tregambi, C., Montagnaro, F., Salatino, P., Chirone, R., Solimene, R. (2021) Improving the performance of calcium looping for solar thermochemical energy storage and CO_2 capture. *Fuel*, 298, 120791.

[7] Tregambi, C., Di Lauro, F., Pascual, S., Lisbona, P., Romeo, L.M., Solimene, R., Salatino, P., Montagnaro, F. (2023) Solar-driven calcium looping in fluidized beds for thermochemical energy storage. *Chem. Eng. J.*, 466, 142708.